Ti alloy with enhanced machinability in UAT turning

Ti Alloy with Enhanced Machinability in UAT Turning

AGOSTINO MAUROTTO, CARSTEN SIEMERS, RIAZ MUHAMMAD, ANISH ROY, and VADIM SILBERSCHMIDT

Metastable β-titanium alloys such as Ti 15V 3Al 3Cr 3Sn are of great technological interest thanks to their high fatigue strength-to-density ratio. However, their high hardness and poor machinability increase machining costs. Additionally, formation of undesirable long chips increases the machining time. To address those issues, a metastable β-titanium alloy (Ti 15V 3Al 3Cr 2Zr 0.9La) with enhanced machinability was developed to produce short chips even at low cutting speeds. A hybrid ultrasonically assisted machining technique, known to reduce cutting forces, was employed in this study. Cutting force components and surface quality of the finished work-pieces were analyzed for a range of cutting speeds in comparison with those for more traditional Ti 15V 3Al 3Cr 3Sn. The novel alloy demonstrated slightly improved machining characteristics at higher cutting speeds and is now ready for industrial applications.

I. INTRODUCTION

LIGHT-WEIGHT materials such as titanium alloys have gained popularity in modern aerospace structures due to their excellent mechanical and physical properties. Some of the well-documented advantages of titanium alloys are high strength-to-weight ratio, relatively low density, excellent corrosion resistance, and a low modulus of elasticity. However, titanium alloys have been classified as difficult to machine due to their physical properties.[1] Also, their chemical reactivity with tool materials and consequent adhesion to the cutting tool during machining can lead to excessive tool chipping and/or premature tool failure and poor surface finish. Titanium alloys also maintain their high strength levels at elevated temperature in addition to their low modulus of elasticity and thermal conductivity. These characteristics cause high temperatures at the cutting interfaces during machining and result in higher tool wear rates.[2] Finally, automated machining of such alloys is almost impossible due to formation of long chips, especially during drilling and turning operations. As a result, during component manufacturing, the cutting process has to be interrupted as often as necessary to remove chips from the process zone to avoid poor surface quality or fatal tool failure.[3]

Metastable-β alloys like Ti 15V 3Al 3Cr 3Sn (Ti-15-3-3-3), Ti 10V 2Fe 3Al (Ti-10-2-3), or Ti 5Al 5V 5Mo 3Cr 0.5Fe (Ti-5-5-5-3) are nowadays intensively investigated, since their fatigue strength can be raised up to 800 MPa by age-hardening.[4] Those beneficial effects identify this family of alloys as one of the most important for manufacturing processes since its widespread adoption in aerospace industry. However, titanium alloys show poor thermal conductivity and high chemical reactivity with tool materials. Those effects impair machinability at high cutting speeds, while at low-to-medium cutting speeds, those alloys produce long helicoidal chips, which are undesirable in modern automated machining processes.[5] Production costs could be reduced by improving the material removal rate (MRR) and by reducing the chip length and, hence, enable automated manufacturing.

In machining, three different types of chips are known to form, namely, continuous chips having a constant chips thickness, segmented chips showing a saw-tooth-like geometry, and completely separated segments.[6] During machining, Ti-15-3-3-3 shows a change from continuous to segmented chip formation for both solution-treated and aged states; this change depends on cutting parameters.[7] For industry-relevant cutting speeds, segmented chips are obtained.[8] This results in high friction at the flank and rake faces of the tool. As a result, concentrated hot spots appear at the interface between the tool and the chip. Segmented chip formation can be explained as follows: during the beginning of the cut, the tool penetrates the work-piece damming the material in front of the tool. The initiated plastic deformation is concentrated in a narrow zone, the so-called *primary shear zone*. Most of the energy used for plastic deformation is transformed into heat in this zone, leading to local softening of the material and, hence, to formation of segmented chips (see Figure 1). The strain level in shear bands can easily exceed 800 pct at strain rates up to 10^7 s^{-1}; the temperature in shear bands in titanium alloys can exceed 1173 K (900 °C). The chip is afterward guided along the rake face of the tool, the so-called secondary shear zone. The

AGOSTINO MAUROTTO, Research Associate, is with the Nuclear Advanced Manufacturing Research Centre, University of Sheffield, S60 5WG Rotherham, U.K. Contact e-mail: a.maurotto@namrc.co.uk CARSTEN SIEMERS, Senior Research Scientist, is with the Institut für Werkstoffe, Technische Universität Braunschweig, 38106 Braunschweig, Germany. RIAZ MUHAMMAD, Associate Professor, is with the Department of Mechanical Engineering, CECOS University of IT and Emerging Sciences, Peshawar, KPK, Pakistan. ANISH ROY, Senior Lecturer, and VADIM SILBERSCHMIDT, Professor, are with the Wolfson School of Mechanical and Manufacturing Engineering, Loughborough University, Loughborough LE11 3TU, U.K.

temperature at the end of the secondary shear zone can also rise to more than 1173 K (900 °C).[9]

To improve machinability, lanthanum was selected as an alloying element because of its low solubility in titanium at room temperature. During crystallization of a related alloy, it precipitates mainly along the grains boundaries. High temperatures observed in shear bands were considered sufficient to soften the La particles located in them. Hence, in the process of the tool's progress, adhesion between the segments is strongly reduced; as a result, chips separate along the related shear bands so that chip fragmentation is observed.[9]

Due to high reactivity of Ti at high temperatures, machining of titanium is generally carried out under a flow of coolant. In recent times, increasing environmental concerns resulted in questioning of the use of cutting fluids in metal cutting. Their handling and disposal can form the major part in overall machining costs, to the point that costs related to cutting fluids can exceed those of cutting tools. Thus, partial or total elimination of cutting fluids is seen as an important challenge. Dry machining is hence of great interest, since it removes the need for cutting fluids and lubricants addressing the environmental concerns.[10] However, the need to avoid excessive heat generation in the cutting tool and, consequently, rapid tool wear prevents achievement of high MRR levels in dry cutting.[11] Low cutting speeds are generally disadvantageous, resulting in unwanted longer chips, and high cutting forces caused by hardness of the machined alloys; they can trigger undesirable vibrations, ultimately accuracy of the finished workpiece.[12]

For those reasons, a hybrid machining technique—ultrasonically assisted turning (UAT)—was selected for the experiments. For these tests, the cutting tool was vibrated at a frequency of 17.8 kHz. In the previous studies,[13,14] a transition from a ductile cutting regime to a brittle one was observed at higher magnitudes of the depth of cut a_p when ultrasonic vibration was superimposed on the movement of the cutting tool when machining intractable materials. This effect was used to demonstrate a large range of beneficial effects in the machining of difficult-to-machine materials[15–18] Drastic changes in the elasto-plastic behavior of the material were observed[19,20] along with changes in interfacial processes, in which dry static friction at the boundary between the tool and the work-piece transformed into dynamic viscous friction in the presence of ultrasonic vibration.[21]

In order to preserve an acceptable MRR at low cutting speeds, a_p should be increased. However, cutting forces are proportional to a_p, but they can be reduced thanks to the hybrid machining. This effect is especially pronounced when the vibration of the tool is along the cutting direction.[16,22]

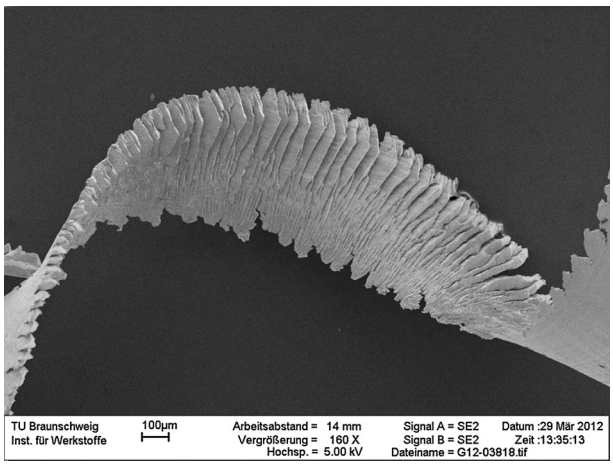

Fig. 1—SEM Image of Ti segmented chip.

II. EXPERIMENTAL SETUP

To perform the UAT tests, a Harrison 300 lathe was adequately modified to accommodate an ultrasonic cutting head. In this setup, functionality for conventional turning was preserved with the flexibility of switching between the conventional and ultrasonic cutting regimes during a single turning operation.[17] A standard Langevin-type piezoelectric transducer[23] was coupled with an aluminum concentrator and a titanium tool holder to form the ultrasonic cutting head. Titanium, offering a favorable strength-to-mass ratio, was preferred for the tool holder, since an additional mass attached to the concentrator shifts the resonating frequency and amplitude of the transducer.[24]

A specially designed tool-post attachment was used to fix the cutting head to the cross slide of the lathe. A care was taken to ensure the maximum rigidity of the assembly and reduce a displacement of the head when subjected to high cutting forces. A Kistler 9257A three-component dynamometer was used to measure the average cutting-force components up to 5 kN with a maximum frequency of 2.5 kHz (Table I).[25]

The vibration amplitude was monitored during the cutting process with a non-contact measurement technique involving a Polytech OFV-3001 laser vibrometer. During the entire cutting process, the amplitude of the cutting tool was acquired. It was observed that the resonance-frequency response of the system was sufficiently broad to be insensitive to small variations, which are inherent to cutting operations. For the machining experiments reported in this work, the vibration resonance frequency was 17.8 kHz with peak-to-peak amplitude of 20 μm.

Table I. Cutting-Tool Specification[27]

Tool maker	SECO
Tool part number	DNMG 150608 MF1 CP500
Tool material	micro-grain cemented carbide
Coating	(Ti,Al)N-TiN
Tool nose radius, r_n (mm)	0.8
Nose angle	55 deg
Cutting edge radius (μm)	25
Rake angle	14 deg 6′
Chamfer angle	0 deg

An accurate control on the depth of cut a_p during the machining operation is of paramount importance to compare machining results for both alloys A and B—in conventional and ultrasonically assisted turning. This was ensured with the use of a micrometric dial gage (Figure 2) with an accuracy of ±10 μm. Such precision is deemed appropriate for the measurement needs.[18]

A. *Cutting Tool*

UAT is a tough cutting technique for conventional cutting tools. The intermittent contact between the tool and the work-piece, and high temperatures can easily bring the tools beyond their design limits. High vibration frequencies are very demanding to the tool material's resistance to fatigue. For this reason, a micro-grain structure of the tool optimized for intermittent cutting was selected along with a larger, thus, more robust, nose radius.

Coated micro-grained cemented carbide tools with a node radius of 0.8 mm (Table I) were used in all the experiments reported in this paper. Previous experiments suggested that a PVD-coated tool with a ceramic layer of (Ti-Al)N over a primer layer of TiN offered the highest resistance to wear, while uncoated tools did not withstand the cutting operation in UAT for more than a couple of seconds. The presence of Al in the coating leads to formation of a glassy alumina-oxide protective layer on the surface of coating, thus, increasing the tool resistance at high operating temperatures.[26]

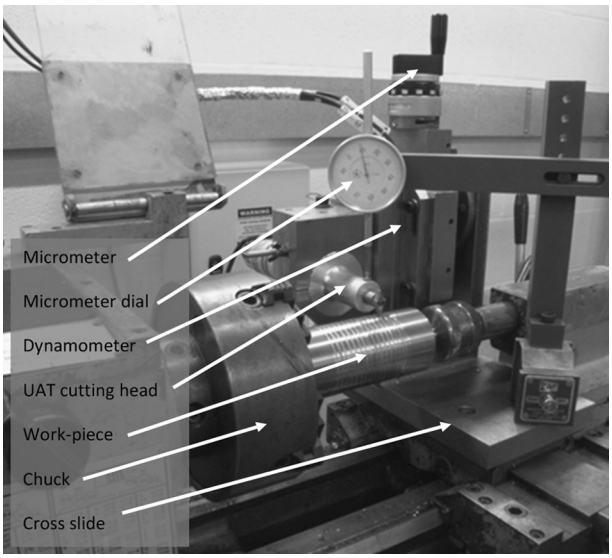

Fig. 2—UAT lathe machining Ti 15-3-3-3 alloy.

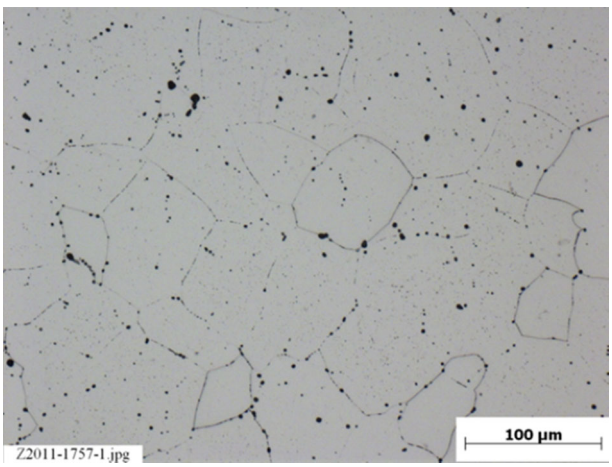

Fig. 3—Microstructure for Alloy B.

B. *Work-Piece Materials*

Both alloys investigated in this study—Ti 15V 3Al 3Cr 3Sn (alloy A) and Ti 15V 3Al 3Cr 2Zr 0.9 La (alloy B)—have similar β-transus temperatures and can be age-hardened to more than 1100 MPa (UTS). The presence of strong β-stabilizing alloying elements, such as V and Cr as well as α-stabilizer Al renders alloys sensitive to solution and aging treatments. As Sn and Zr only show a limited influence on the β-transus temperature, they act as solid-solution hardeners. In alloy B, Zr was used instead of Sn to avoid formation of La_xSn_y intermetallic phases with high melting temperatures.[28]

The alloys were produced from the following raw materials: CP-Titanium Grade 2 following ASTM B348, two commercially available pre-alloys 85V 15Al and 50V 40Cr 10Al (provided by the GfEMetalle and Materialien GmbH, Nuremberg, Germany) and elementary La (purity 99.9+ pct), Sn (purity 99.99 pct) and Zr (purity 99.95 pct) (provided by ChemPurFeinchemikalien und Forschungsbedarf GmbH in Karlsruhe, Germany). To ensure the same initial conditions, the alloys were molten and twice re-molten in a laboratory-size vacuum arc furnace (PB-CHM) with a capacity of approx. 400 g titanium. A care was taken to ensure sufficient homogeneity of the produced materials. After the third melting step, the alloys were cast into a water-cooled crucible with diameter 30 mm. The resulting bars were then annealed at 1063 K (790 °C) for 30 minutes in air followed by air cooling.

During the cooling phase, the titanium matrix crystallizes (along with the alloying elements) into grains leaving the majority of rare earth metal atoms in the remaining liquid phase. Once the matrix is fully crystallized, the rare element remains trapped on the grain boundaries, finally crystallizing at lower temperatures.

The surface layers containing α-phase were removed by wet machining at low speeds to avoid new surface contamination. In the solution-treated state, the alloys consisted of only β-phase in case of alloy A and β-phase and La-/La_2O_3-particles in case of alloy B. In metallographic analyses, alloy B presented La/La_2O_3 precipitates as black dots along the grains boundaries (Figure 3). The solution-treated state was chosen for our experiments, as the machinability of this state is the most difficult due to a low Young's modulus and, thus, low stiffness of the bar, resulting in spring-back of the work-piece material causing tool rubbing, chatter, and additional tool wear.

The relevant physical and mechanical properties of both alloys are summarized in Tables II and III.[29] Due to a relatively small size of the obtained samples

Table II. Mechanical Properties of Alloy A[40]

Work-piece material	Ti 15V 3Al 3Cr 3Sn
Producer	TU Braunschweig
Heat treatment	solution treated
Young's Modulus, E (GPa) at RT	84 ± 2
Density, ρ (kg/m^3)	4760
Thermal conductivity, k (W/km)	8.10
UTS (MPa)	830 ± 10
Sample size, diameter-length (mm)	30 to 50

Table III. Mechanical Properties of Alloy B[40]

Work-piece material	Ti 15V 3Al 3Cr 2Zr0.9La
Producer	TU Braunschweig
Heat treatment	solution treated
Young's Modulus, E (GPa) at RT	78 ± 4
Density, ρ (kg/m^3)	4730
Thermal conductivity, k (W/km)	approx. 7.5
UTS (MPa)	740 ± 30
Sample size, diameter-length (mm)	30 to 50

Table IV. Cutting Parameters

Cutting speed, V (m/min)	10, 30, 60
Feed, f (mm/rev)	0.1
Depth of cut, a_p (μm)	200
Coolant	none

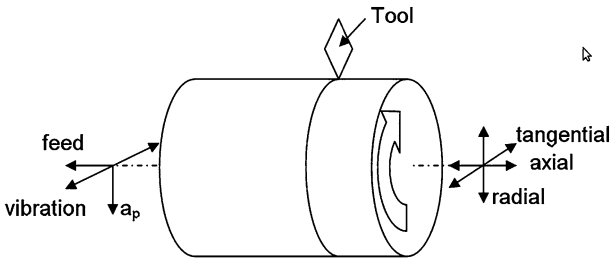

Fig. 4—Relative positions of cutting tool and work-piece together with principal directions.

(diameter 30 mm, length 50 mm), it was necessary to keep the duration of experimental runs below 60 seconds of continuous cutting in order to avoid heating up of these small samples and edge effects.

C. *Cutting Parameters*

Each experimental run in the cutting experiments was repeated five times to check the consistency of the results. Details of the machining parameters are available in Table IV.

For the experimental tests, the cutting insert was mounted orthogonal to the work-piece with its rake face aligned along the tangential direction (Figure 4). Each experimental run lasted approximately 60 seconds, of which first 10 seconds were used to set a_p to the desired value. Conventional turning was then started for 30 seconds. Next, the ultrasonic generator was switching on without stopping the machining operation, effectively transforming the system into a UAT system. During this time, a transient regime was observed, while the system reached the maximum amplitude of vibrations. Although the transient regime lasted for less than 2 seconds, it was considered prudent to allow 5 seconds for the system to completely stabilize at the standard operation conditions. Cutting then continued for 30 seconds before vibration was switched off, and the conventional-turning regime recovered; following that, the cutting tool was disengaged from the work-piece, and the machine was then stopped.

Before each experimental run, the tool was allowed to cool to room temperature. This helped to mitigate excessive heat build-up in the tool during the machining operations, which may lead to premature tool failure.[18]

Increasing the cutting speed at a fixed a_p increases the MRR; however, it is not possible to increase the cutting speed indefinitely, especially in UAT. From a 1-D theory of ultrasonic cutting, it is possible to derive a relation among the amplitude of oscillations of the tool, the frequency, and the rotational speed of the work-piece at which the UAT process will be effective. In order to achieve the force reduction, it is necessary that there is complete separation between the tool and the work-piece in each vibratory cycle of the tool.[16,21] The critical cutting velocity is derived to be

$$V_c = 2\pi af, \qquad [1]$$

where a and f are, respectively, the amplitude and frequency of the ultrasonic vibration.[21] The cutting speed V is related to the rotational speed by the following expression:

$$V = \pi nD, \qquad [2]$$

where D is the diameter of the machined work-piece, and n is the rotational speed of the chuck.

Due to small dimensions of the cutting samples (D = 30 mm), a single depth of cut of 0.2 mm was selected to be a representative level. A low feed rate of 0.1 mm/rev was used to emulate machining conditions in finishing steps, which are generally used for these intractable alloys.[2]

Cutting forces imposed on the tool were measured for CT and UAT at a_p = 0.2 mm for various levels of cutting speed (V = 10, 30, 60 m/min). A cutting velocity of 60 mm/min corresponds to the calculated critical velocity V_c = 55 to 65 m/min (calculated for vibration amplitude between 8 and 10 μm and frequencies between 17.8 and 18 kHz) (Eq.[1]). However, due to the presence of spurious vibrations (radial–axial–torsional) alongside the tangential one, only a reduction in the efficiency of UAT is expected at this speed.

D. *Surface Roughness*

A non-contact, three-dimensional interferometry profiler ZYGO 3D-NV5000-5010 was used in all the surface roughness measurements. In order to reduce the error

associated with the measurement, three measuring points were taken six times for each machined surface diameter. The obtained data were post-processed using Taylor Hobson Talymap Platinum 3D analysis software.

An amplitude, spacing, and hybrid parameters were chosen to characterize the quality and roughness of 3D surface of the machined work-piece. The depth of cut in those studies was 0.2 mm at the three cutting speed; the observed trends are believed to be characteristic for other depths of cut.

III. RESULTS

The largest reduction in cutting forces thanks to UAT was expected to be in the tangential component, since the primary vibration direction was in that direction.[30] The relatively large nose radius of the cutting tool used coupled with the relatively small a_p resulted in a very low axial force, which was not reported in the examined results.[18]

The tangential and radial components of the cutting force for alloys A and B are compared in Figure 5 and Table IV for the same depth of cut of 0.2 mm at different cutting speeds. Variability of the measured data is represented with error bars in the figures

While cutting alloy B at a speed of 10 m/min (Figure 1), the cutting force in conventional turning appeared to be similar to that for alloy A. From a more detailed analysis (Table IV), a small reduction in both the radial and tangential components of the cutting force, even if of little significance for cutting, was observed and explained by the reduced mechanical properties of alloy B. When machining in UAT, alloy B presented an unexpected behavior with a large increase in the cutting force to values similar to those observed in CT. An increase of the radial component of the cutting force was observed in alloy B when cutting in UAT (Table IV).

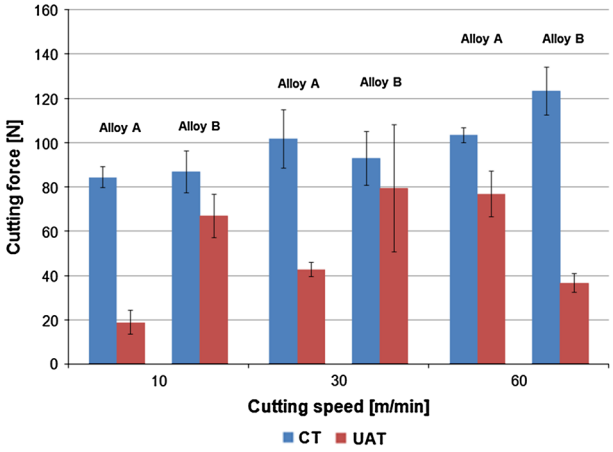

Fig. 5—Comparison of cutting forces.

At a cutting speed of 30 m/min (Figure 1), a difference between the levels of cutting force for the alloys in CT remained insignificant. A general increase of noise in the recorded data was also observed, which further reduced the significance of the observed differences. Similar behavior to that at 10 m/min was observed for the radial component in UAT, with a slightly higher recorded force for alloy B. High levels of noise were recorded for the radial cutting force component for alloy B in UAT, which appeared to be significantly higher than that for alloy A (Table IV).

The machining test at a speed of 60 m/min showed lower values of noise compared to the levels observed at the low end of cutting speed. Results for conventional turning were consistent, with no differences between behaviors of alloys A and B. The latter was observed to have a higher cutting force than the former for both the radial and tangential components when machined in conventional turning. An opposite was true for UAT. Reduced levels of noise were also observed for UAT of alloy B, with levels similar to those for alloy. Table V summarizes the observed values.

A. *Surface Finish*

The aerospace applications, for which the studied alloys are used, require high surface quality in the finished components. It is well known that poor surface characteristics imply a reduction in fatigue resistance of machined components.[1,31] Thus, surface quality can be considered to be one of the crucial factors in metal cutting. A direct way of measuring the surface quality is the measurement of surface roughness using non-contact experimental techniques. Commonly, optical or laser profilometry is used in surface evaluation and assessments by using amplitude and spacing parameters.[32] The interferometry-based Zygo was used to

Table V. Cutting Forces for Alloys A and B in CT and UAT at a_p = 0.2 mm and Various Speeds

Cutting Speed (m/min)	Cutting Force Components (*N*)							
	CT				UAT			
	Tangential		Radial		Tangential		Radial	
	Alloy A	Alloy B	Alloy A	Alloy B	Alloy A	Alloy B	Alloy A	Alloy B
10	84.1 ± 2.5	70.3 ± 6.4	53.5 ± 3.9	51 ± 6.8	10.7 ± 1.7	15.6 ± 1.9	15.6 ± 5.1	65.2 ± 9.6
30	82.6 ± 10	70.7 ± 8.1	59.3 ± 8.6	60.3 ± 9.1	23.5 ± 2.5	27.3 ± 6.3	35.8 ± 2.0	74.6 ± 28
60	82.2 ± 2.0	91.7 ± 5.1	62.7 ± 2.6	82.4 ± 9.4	46 ± 7.0	35.9 ± 2.9	61.5 ± 7.7	50.6 ± 3.0

Table VI. Roughness Parameters for Alloys A and B in CT and UAT at a_p = 0.2 mm and Various Speeds

Cutting Speed (m/min)	Rz (μm)		Ra (μm)		Rsk		Rku		PSm (μm)		Sq (μm)		Spd	
	A	B	A	B	A	B	A	B	A	B	A	B	A	B
10 CT	0.87	0.93	0.09	0.12	1.13	0.18	2.68	0.68	31.70	19.70	0.44	0.33	2183	24258
10 UAT	0.40	2.93	0.08	0.55	0.25	−0.95	0.52	6.82	1.79	43.00	0.12	1.86	9008	1367
30 CT	2.88	2.10	0.51	0.35	0.33	−0.57	2.57	5.99	16.30	46.80	1.46	1.73	4947	1515
30 UAT	2.57	2.33	0.47	0.44	0.32	−0.04	2.46	3.58	2.46	55.00	1.27	1.74	13558	2297
60 CT	2.55	2.27	0.42	0.40	2.40	−0.41	2.99	3.89	13.27	27.13	1.18	1.60	6201	436
60 UAT	2.68	2.61	0.47	0.47	0.30	0.41	2.6	4.80	19.70	32.10	1.24	1.34	8267	1907

acquire 2D maps of the finished surface of the work-piece. A care was taken to generate a sufficient number of points to provide a representative dataset. The obtained results are summarized in Table VI.

The main linear roughness parameters, Rz and Ra, showed that alloy B performed significantly worse than alloy A at the lowest cutting speed used. Lower roughness was observed for alloy B at high speed and in UAT. The skewness parameter Rsk demonstrated a predominance of valleys for Alloy B at all but the highest speed in UAT, while the kurtosis parameter Rku was slightly increased for alloy B, indicating steeper profiles.

The spacing parameter PSm showed higher values for alloy B, especially for UAT. Areal-roughness measurements provided similar results for both alloys A and B at all but the lowest cutting speed. Interestingly, the peak density parameter Spd for alloy B was generally lower than for alloy A at all but 10 m/min cutting speed, showing a reduced density of peaks, especially in CT.

IV. DISCUSSION

Alloy B was originally developed to improve the poor chip breakage characteristics typical for Ti alloys. The desirable interrupted chip formation was not observed at 10 m/min and 30 m/min, and long helicoidal chips, typical for beta-Ti alloys,[2] were formed during machining of both alloys. At the highest speed of 60 m/min, alloy B showed shorter chip formation, albeit not consistently. It is, thus, believed that the alloy requires cutting speeds higher than 60 m/min in order to achieve a fully interrupted chip. Both alloys showed chip segmentation at cutting speeds exceeding 60 m/min.

When the collected cutting results were organized in a cumulative graph, differences between the two alloys became evident (Figure 6). It is observed that alloy B performs better than alloy A at 60 m/min showing a significant force reduction even at cutting speeds close to the critical velocity. The observed cutting force reduction could be explained by cumulative effects of successive plastic deformations that the work-piece undergoes under UAT.[21] A smaller but still significant role is possibly played by the ultrasonic softening process.[33,34] It is known that crystalline defects in metals can absorb selectively ultrasonic energy and become activated. It is possible that La precipitates acted as a selective absorber of ultrasonic energy, reducing the energy needed for its deformation.

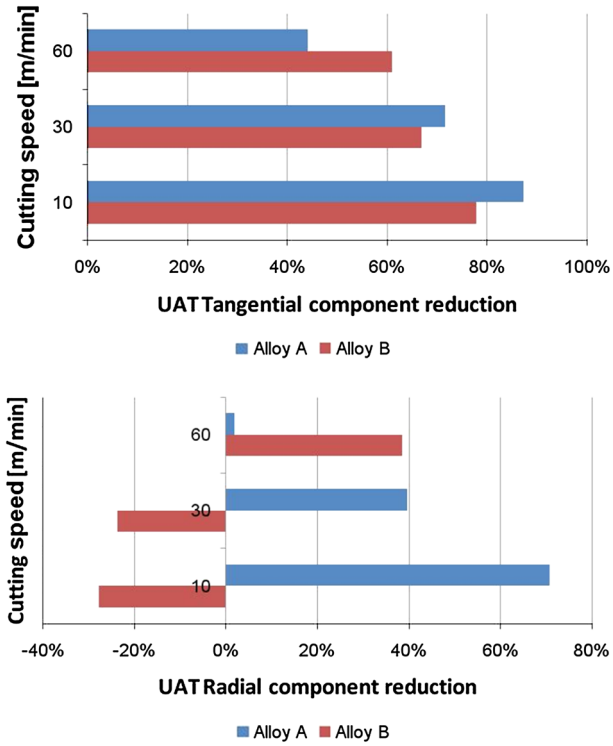

Fig. 6—Reduction of tangential and radial components of cutting force for alloys A and B at different cutting speeds (a_p = 0.2 mm, f = 0.1 mm/rev).

Higher radial components of the cutting force in UAT than in conventional machining show significantly different behaviors of alloy B when machined ultrasonically. This dramatic behavior has not been observed before in machining of Ti alloys and could be linked to the presence of lanthanum in the alloy. Faster-than-normal tool wear was also observed at all the studied cutting speeds when machining alloy B with increased heat build-up during the machining operations. This is consistent with high chemical reactivity of La precipitates between the alloy grains.

It is evident that at cutting speeds close to the critical velocity, alloy B was significantly softer than alloy A. This could be explained by higher temperatures reached in the cutting zone. It is not uncommon for Ti alloys to easily reach temperatures over 1173 K (900 °C) in the cutting zone.[35–37] The reached temperatures are close to the melting point of the lanthanum particles, which could ultimately soften and reduce the cohesion between the

grains. The presence of an almost-fluid bed at the inter-grain boundaries would reduce the energy needed to displace the crystal ultimately leading to a reduction in the energy needed to deform the material.[38] Yet, the presence of particles weakening the grain boundaries could lead to a reduction of the alloy's resistance to crack propagation.

The universally used center-line average Ra showed a similar behavior for alloy A in CT and UAT at all the cutting speeds studied. Alloy B performed significantly worse in UAT at low cutting speeds. The differences between the alloys became more obvious when considering the area roughness Sq: alloy A performed better in UAT at all but the highest cutting speed, while alloy B demonstrated an opposite trend. Alloy B's area roughness was better in UAT at the highest cutting speed, thus, showing that the alloy is more suited for high-speed machining. This result was consistent with the presence of La, which would be generally more effective at higher temperatures of the deformation area.[38] Limitations of the current setup, however, prevented implementation of tests at higher cutting velocities. The tribological properties of the machined surfaces of the studied alloys were also different: a skewness parameter of the profiles in UAT for alloy A was significantly different from that of alloy B; alloy B showed highly leptokurtic surfaces in both CT and UAT regimes. Generally, cutting of alloy B at high speeds resulted in a lower density and height of peaks; the generated surface appeared to show a predominance of valleys. Spacing of surface defects was also increased in alloy B, ultimately resulting in a lower number of deviations from the mid-line with large spacings between each other.

V. CONCLUSIONS

The modified alloy did not appear to exhibit the desired chip-breakage behavior at all the cutting speeds analyzed. Addition of lanthanum that precipitated as inter-grain impurity significantly changed the response to ultrasonically assisted turning. The combination of lower thermal conductivity and higher cutting forces for alloy B was expected to increase temperatures in the shear band and deformation area, ultimately hastening softening of La particles. In order for this process to happen, a sufficient temperature must be achieved in the process zone to allow softening of the La particles. The performed tests showed that a cutting speed of 60 m/min was not sufficient to trigger the phenomena even in the presence of added energy in UAT.

The cutting forces observed in machining of alloy B differed significantly from those observed in the machining of alloy A. Minute variations of the alloying elements and impurities added had a noticeable impact on the magnitude of cutting force components in both conventional and ultrasonically assisted turning processes. It was proven that the presence of low melting inter-grain elements affected mechanical properties of the alloy and modified their machinability. Differences both in alloying elements and the presence of La precipitates changed extensively mechanical and machining behaviors of alloy B when compared to alloy A.

The primary cause of heat generation in metal cutting is the plastic deformation work in the primary and secondary shear zones. Contribution of friction between tool and work-piece is generally assumed to be minimal and below 10 pct of the total.[39] Increasing the plastic deformation rate (by increasing cutting speed) directly increases the heat generated in the shear zone. This, together with the low thermal conductivity of Ti alloys, has the effect of increasing cutting zone temperature.

Therefore, higher cutting speeds could improve the interrupted chip formation observed in alloy B if the found trend is maintained; however, the effect of the temperature variation in the cutting zone should be considered, since it could weaken the resistance to the cutting tool.

Further studies are necessary to understand mechanisms responsible for different machining characteristics of the two studied alloys in CT and UAT.

ACKNOWLEDGMENTS

Funding from the European Union's Seventh Framework Programme (FP7/2007–2013) under Grant Agreement No. PITN-GA-2008-211536, project MaM-iNa, is gratefully acknowledged.

REFERENCES

1. S. Sun, M. Brandt, and M.S. Dargusch: *Int. J. Mach. Tools Manuf.*, 2009, vol. 49, pp. 561–68.
2. M.J. Donachie: *Titanium A Technical Guide*, ASM International, Materials Park, OH, 2000.
3. C. Siemers, J. Laukart, B. Zahra, J. Rösler, Z. Spotz, and K. Saksl: *Development of Advanced and Free-Machining Alloys by Micrometer-Size Particle Precipitation*, Materials Science Forum, Trans Tech Publications, Zurich, 2011, vol. 690, pp. 262–65.
4. G. Lütjering and J.C. Williams: *Titanium*, Springer Verlag, Berlin, 2003.
5. N. Zlatin and M. Field: in *2nd Int. Conf. Titan. Sci. Technol.*, R.I. Jaffee and H.M. Burte, eds., Metallurgical Society of AIME, New York, 1973, p. 489.
6. R. Komanduri and R.H. Brown: *ASME J. Eng. Ind.*, 1981, vol. 103, pp. 33–51.
7. P. Rokicki, K. Nowag, Z. Spotz, L. Fusova, K. Saks, R. Ghisleni, and C. Siemers: *Rudy i metale nieżelazne*, 2010, vol. 55, pp. 452–56.
8. C. Siemers, F. Brunke, J. Laukart, M.S. Hussain, J. Rösler, K. Saksl, and B. Zahra: *Proc. COM 2012*, Niagara Falls, 2012.
9. J. Rösler, M. Bäker, and C. Siemers: in *High Speed Machining*, H.-K. Tönshoff and F. Hollmann, eds., VCH-Wiley, Weinheim, 2005, pp. 492–514.
10. G. Byrne and E. Scholta: *CIRP Ann. Manuf. Technol.*, 1993, vol. 42 (1), pp. 471–74.
11. K. Weinert, I. Inasaki, J.W. Sutherland, and T. Wakabayashi: *CIRP Ann. Manuf. Technol.*, 2004, vol. 53, pp. 511–37.
12. F. Klocke and O. Rubenach: *Ind. Diam. Rev.*, 2000, vol. 60, pp. 227–39.
13. J. Devine: *Soc. Adv. Mater. Process Eng.*, 1979, vol. 10, pp. 485–96.
14. J. Kumabe, K. Fuchizawa, T. Soutome, and Y. Nishimoto: *Precis. Eng. Nanotechnol.*, 1989, vol. 11, pp. 71–77.
15. D. Brehl and T. Dow: *Precis. Eng.*, 2008, vol. 32, pp. 153–72.
16. V.I. Babitsky, A.V. Mitrofanov, and V.V. Silberschmidt: *Ultrasonics*, 2004, vol. 42, pp. 81–86.
17. A. Maurotto, A. Roy, V.I. Babitsky, and V.V. Silberschmidt: *Proc. 4th CIRP HPC (CIRPHPC2010)*, Gifu, Japan, 2010.

18. A. Maurotto, A. Roy, V.I. Babitsky, and V.V. Silberschmidt: *Solid State Phenom.*, 2012, vol. 188, pp. 330–38.
19. M. Demiral, A. Roy, and V.V. Silberschmidt: *Comput. Mater. Contin.*, 2010, vol. 19, pp. 199–216.
20. R. Muhammad, A. Maurotto, A. Roy, and V.V. Silberschmidt: *Appl. Mech. Mater.*, 2011, vol. 70, pp. 315–20.
21. V.K. Astashev and V.I. Babitsky: in *Ultrasonic Processes and Machines*, V.I. Babitsky and J. Wittenburg, eds., Springer, New York, 2007.
22. A.R.C. Sharman, P. Bowen, and D.K. Aspinwall: *Ultrasonic Assisted Turning of Gamma Titanium Aluminide*, Rolls-Royce PLC, London, 2001.
23. E. Moreno, P. Acevedo, M. Fuentes, A. Sotomayor, L. Borroto, M.E. Villafuerte, and L. Leija: *2nd Int. Conf. Electr. Electron. Eng.*, 2005, pp. 393–95.
24. A.I. Markov: *Russ. Eng. Res.*, 1996, vol. 16, pp. 26–31.
25. Kistler: http://www.kistler.com/, Accessed March 2011.
26. A. Joshi and H.S. Hu: *Surf. Coat. Technol.*, 1995, vols. 76–77, pp. 499–507.
27. SECO: SECO-Web Catalog [Online], http://ecat.secotools.com/, Accessed March 2011.
28. M.S. Hussain, C. Siemers, and J. Rosler: *J. Mater. Manuf. Process.*, 2013, vol. 28, pp. 545–49.
29. B. Zahra, F. Depertori, C. Siemers, and J. Rösler: *Proc. 12th World Conf. Titan. (Ti-2011)*, Beijing, China, 2011.
30. A. Maurotto, R. Muhammad, A. Roy, and V.V. Silberschmidt: *Ultrasonics*, 2013, vol. 53, pp. 1242–50.
31. T.H.C. Childs, D. Richings, and A.B. Wilcox: *Int. J. Mech. Sci.*, 1972, vol. 14, pp. 359–68.
32. E.S. Gadelmawla, M.M. Koura, T.M.A. Maksoud, I.M. Elewa, and H.H. Soliman: *J. Mater. Process. Technol.*, 2002, vol. 123, pp. 133–45.
33. F. Blaha and B. Langenecker: *Naturwissenschaften*, 1995, vol. 77, p. 536.
34. B. Langenecker: *IEEE Trans. Sonic Ultrason.*, 1966, vol. 13, pp. 1–8.
35. S. Hong and Y. Ding: *Int. J. Mach. Tools Manuf.*, 2001, vol. 41, pp. 1417–37.
36. P.-J. Arrazola, A. Garay, L.-M. Iriarte, M. Armendia, S. Marya, and F. Le Maitre: *J. Mater. Process. Technol.*, 2009, vol. 209, pp. 2223–30.
37. C. Leyens and M. Peters: *Titanium and Titanium Alloys: Fundamentals and Applications*, Wiley-VCH, Weinheim, 2003.
38. B. Zahra, C. Siemers, T. Leemet, and J. Rösler: *Proc. 8th Int. Adv. Met. Mater. Technol. Conf. (AMMT'2009)*, Saint Petersburg, Russia, 2009, vol. 1, pp. 461–68.
39. R. Komanduri and Z.B. Hou: *Metall. Mater. Trans. A*, 2002, vol. 33A, pp. 2301–995.
40. R. Wertheim, J. Rotberg, and A. Ber: *CIRP Ann. Manuf. Technol.*, 1992, vol. 41, pp. 101–06.